Damage detection and fatigue strength estimation of carbon fibre reinforced polymers (CFRP) using combined electrical and high-frequency impulse measurements

Daniel HUELSBUSCH [1], Frank WALTHER [1]

[1] Department of Materials Test Engineering (WPT), TU Dortmund University; Dortmund, Germany
Phone: +49 231 7558034, Fax: +49 231 7558029; e-mail: daniel.huelsbusch@tu-dortmund.de

Abstract
CFRP are highly suitable for use in aerospace design for achieving the goal of light-weight construction. However, the use of CFRP poses new challenges to materials testing. New measurement possibilities have to be developed, or existing procedures must be customized to CFRP use. The aim of this study is the in-situ damage detection in quasi-static and cyclic tests and the efficient fatigue strength estimation of CFRP in multiple step tests by using electrical resistance in combination with high-frequency impulse measurements. Quasi-static tensile tests have shown that damage evolution correlates with evolution of AE hit count and change in electrical resistance. Multiple step tests have been applied in order to determine the damage state and evolution as well as to estimate the fatigue properties efficiently, which have been validated by constant amplitude tests. It was found that the developed test approach for CFRP represents a competitive advantage in terms of resource efficiency.

Keywords: Damage detection, Measurement technique, Fatigue, Resource-Efficiency

1. Introduction

Carbon fibre reinforced plastics offer a high potential for lightweight design owing to their high specific strength and stiffness as well as high fatigue resistance compared to metallic materials. The focus on CFRP-oriented research and development is being augmented continuously due to the increased demand of resource conservation and energy efficiency, and the material already finds its utilization in structural applications in automotive and aerospace industry [1]. Fatigue performance of such materials is usually characterized based on Woehler curves, determination of which is time- and cost-extensive. There are no alternative efficient methods available for determination of fatigue performance of laminates [2]. In particular, the in-situ investigation of CFRP components is of great importance, as CFRP components are currently being investigated at defined service intervals making use of ultrasonic and X-ray measurements [3]. Other studies have shown the possibility of in-situ damage detection by combined electrical resistance measurement (ERM) and acoustic emission (AE) measurements [4,5]. This paper investigates the approach for in-situ damage detection and assessment of unidirectional CFRP by simultaneous application of ERM and high-frequency impulse measurement (HFIM), making use of the novel real-time process topography. Focus of this research is the resource-efficient determination of fatigue performance based on damage detection and evolution in multiple step fatigue tests.

2. Testing strategy

Quasi-static tests equipped with ERM and HFIM were carried out to determine the damage evolution and the corresponding damage mechanisms. In HFIM, accumulated acoustic energy and the signal path of the novel three-dimensional process topography was used for the purpose. To evaluate the potential applications of the HFIM and identification of failure mechanisms in CFRP, waveforms were investigated as a function of strain rate and compared and correlated with the ERM and light micrographs. The focus of the cyclic tests was on the assessment of the fatigue properties by means of multiple step test, which has already been

successfully applied to different material groups [6], [7]. However, the previously developed time- and cost-efficient test method for determination of fatigue behaviour of metallic materials, (cf. [8]) is not applicable to CFRP and similar materials due to peculiar damage mechanisms and the absence of "fatigue limit" [2]. By combining multiple step tests (MST) with simultaneous ERM and HFIM measurements, the potential for efficiently determining the fatigue strength of CFRP at $2 \cdot 10^6$ cycles was investigated. Furthermore, the number of cycles per step of MST was varied to reduce the test duration required. The results of the MST were finally validated by constant amplitude tests. All studies were accompanied by analysis of fracture behaviour using light and scanning electron microscopes (SEM).

3. Experimental setup and procedure

The specimens were built out of carbon-fibre-epoxy-prepregs (HS150 EE24 REM). The prepregs were assembled to a six layer unidirectional CFRP system, with fibre content of $62 \pm 3\%$, making use of an autoclave. The specimen geometry was defined according to DIN EN ISO 527-5. Glass fibre reinforced polymers were mounted with epoxy glue on CFRP to make elements for load transmission.

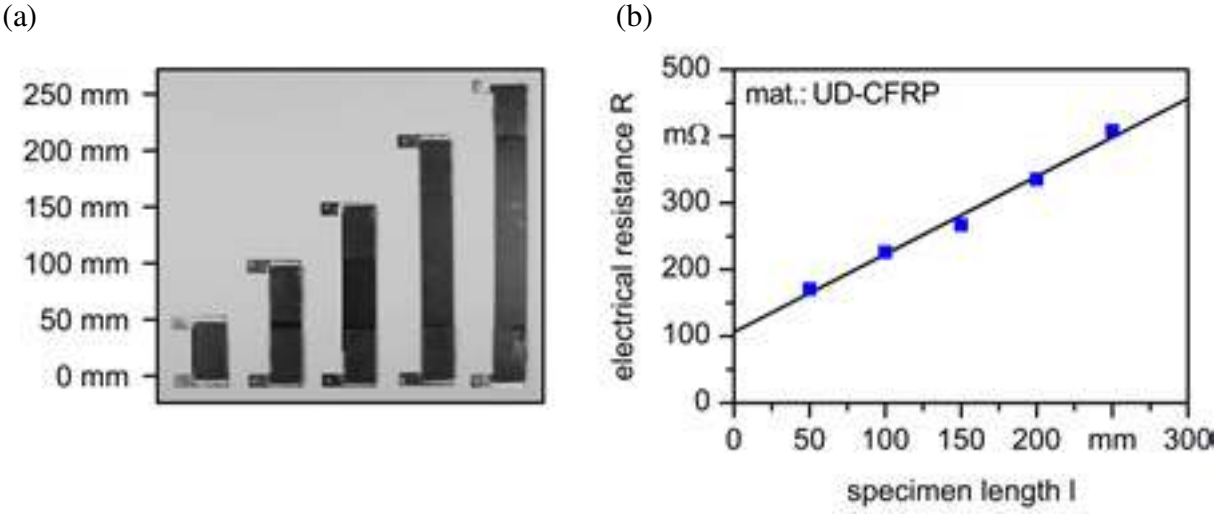

Figure 1. (a) Test specimens and (b) graph to determine the conductor resistance

For reliable high-precision electrical resistance measurement according to DC potential drop method, copper parts were mounted on to the surface and connected to the fibres at the front edge by conductive silver lacquer. The quality of this measurement setup was investigated by measuring the electrical resistance of specimens with varying lengths (Fig. 1 (a)) and extrapolating the resulting graph to a specimen length of 0 mm in order to determine the conductor resistance (Fig. 1 (b)). A value of approx. 106 mΩ could be identified, which corresponds to a sufficient conductor resistance and confirms the reliability of measurement setup. Thermocouples were mounted at three positions (T_1 to T_3) on the specimen surface to measure the specimen temperature as a function of test frequency to identify the frequency, which doesn't lead to a damage-inducing temperature [9]. To get a good connection of the structure-borne sound, the piezo-sensor of the HFIM was fixed on the clamping system. Strain measurements were recorded with a video extensometer (Type: TRViewX, Shimadzu). The testing and measurement setup is shown schematically in Figure 2. Quasi-static tensile tests were carried out at room temperature employing a universal testing system (Type AG-X, Fmax = 100 kN, Shimadzu). The strain rate was varied between $\dot{\varepsilon} = 0.1 \cdot 10\text{-}3\ s\text{-}1$ and $\dot{\varepsilon} = 10 \cdot 10\text{-}3\ s\text{-}1$ to evaluate the suitability of the HFIM (Optimizer 4D, Qass) for detecting the

damage mechanisms. The abort criterion for a standardized stop of the tests was kept at 5% of the maximum force. For the estimation of the fatigue strength, multiple step tests were performed on a servo-hydraulic testing system (Type PC63M, $F_{max} = \pm 63$ kN, Schenck/Instron). Starting at $\sigma_{max,start} = 100$ MPa, the stress amplitude was stepwise increased by $\Delta\sigma_{max} = 100$ MPa after a defined step length ΔN (104 and 103 cycles) until failure. Constant amplitude fatigue tests were used for validation of the estimated fatigue strength. All fatigue specimens were subjected to a stress ratio of R = 0.1 at a frequency of 10 Hz using sinusoidal load-time-function at room temperature.

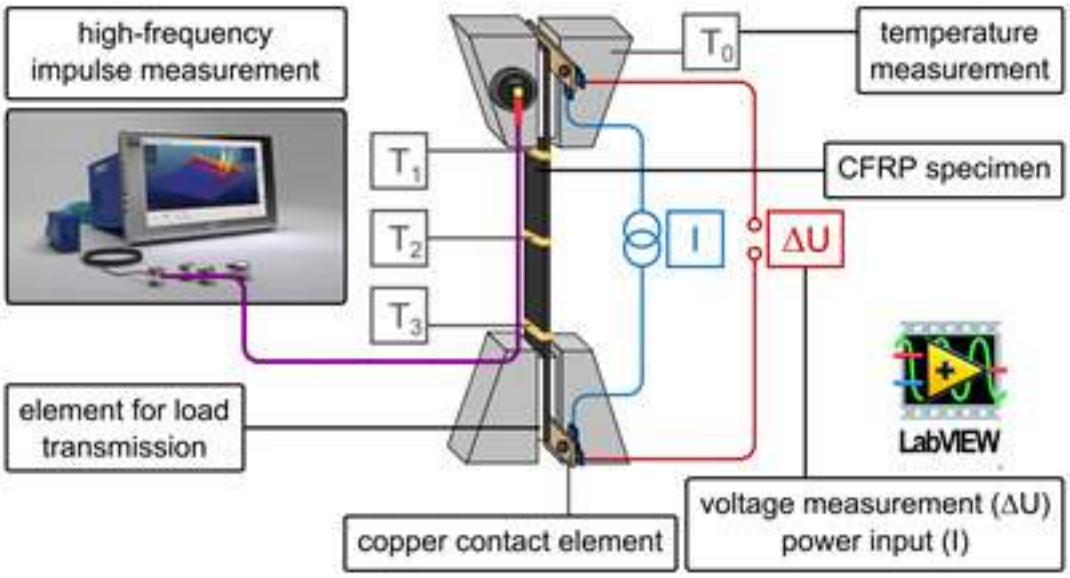

Figure 2. Experimental setup for quasi-static and cyclic tests (schematic)

4. Results and discussion

4.1 Quasi-static Tests

Figure 3 portrays the results of quasi-static tensile tests carried out at a strain rate of $\dot{\varepsilon} = 0.1 \cdot 10^{-3}\ s^{-1}$. The nominal stress σ_n, the electrical resistance R and the nominal sum of acoustic emission AE are displayed for UD-CFRP as a function of total strain ε_t.

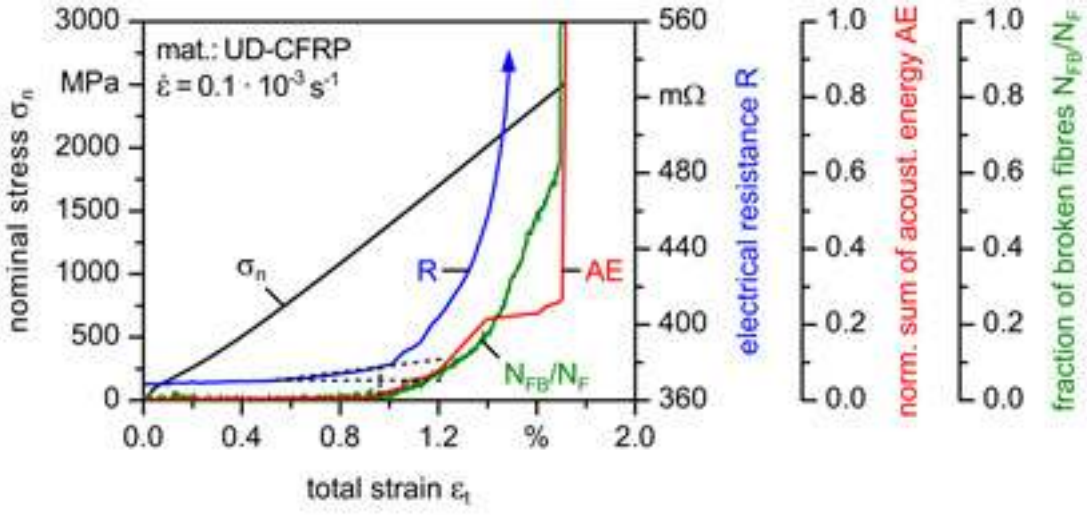

Figure 3. Quasi-static tensile test at $\dot{\varepsilon} = 0.1 \cdot 10^{-3}\ s^{-1}$

The nominal stress increases nearly proportionately with the total strain until specimen's failure at a total strain of 1.7% or 2,500 MPa. The electrical resistance shows a slight linear increase of about 20 mΩ until $\varepsilon_t \approx 1.0\%$, which corresponds to a nominal stress $\sigma_n \approx$ 1,350 MPa. Afterwards, the electrical resistance increases exponentially until failure. The progression of the curve of the nominal sum of acoustic energy is like that of electrical resistance. Up to $\varepsilon_t \approx 1.0\%$ almost no acoustic energy is detected, and experiences a drastic increase after that until failure.

The electrical conduction in the CFRP samples typically runs along the carbon fibres. The linear increase of the electrical resistance R until $\varepsilon_t \approx 1.0\%$ can be attributed to the elastic strain of the carbon fibres. Due to this elongation, the carbon fibres experience a simultaneous reduction in cross-section area A, which leads to a linear increase in R proportional to ε_t [10], which suggests, with a high probability, that there are no fibre cracks until $\varepsilon_t \approx 1.0\%$. At positions of direct contact between adjacent fibres, an electrical conduction can also exist in the longitudinal as well as transverse direction. However, due to the construction of UD-CFRP samples in which the fibres represent parallel-arranged resistors, the transverse conduction can be considered very minute and, therefore, can be neglected. Therefore, it can be assumed that the exponential increase of R after $\varepsilon_t \approx 1.0\%$ is directly related to the number of broken fibres. This assumption can be described mathematically by electromechanical correlation equation (1) by Park et al. [3]. The fraction of broken fibres (N_{FB}/N_F) can be determined by rearranging the equation for N_{FB}/N_F from where the fraction can be determined in terms of total strain, electrical resistance and the proportionality constant (k).

$$\frac{N_{FB}}{N_F} = \frac{1 + k \cdot \varepsilon_t}{1 + \frac{\Delta R}{R_0}} + 1 \qquad (1)$$

The course of the broken fibres over total strain is shown in Figure 3. It can be seen that the damage development in the form of broken fibres correlates well with the changes in electrical resistance R and the normalized sum of the acoustic energy AE. Further, based on Eq. 1 and the fraction of broken fibres, it can be established that 60% of the carbon fibres are broken until $\varepsilon_t = 1.7\%$, followed by rupture. For microstructure-based validation of the test results, the samples at different damage states were examined under light microscope (Fig. 4). In addition to the fibre failures, interference fracture as well as delamination can be seen, but cannot be detected by electric resistance measurement. As the progress of R and AE correlated well, it suggests that both ERM and HFIM detect the same damage mechanisms in the form of fibre cracks [10]. Delamination and matrix cracks do not seem to have been detected.

(a) $\varepsilon_t \approx 1.40\%$ (b) $\varepsilon_t \approx 1.40\%$ (c) $\varepsilon_t \approx 1.55\%$

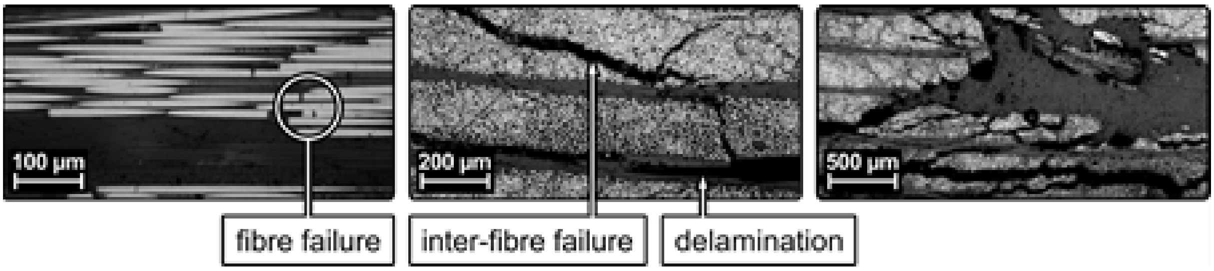

Figure 4. Light micrographs for different strain conditions (a-c)

Figure 5 shows the result of the tensile test carried out at a strain rate of $\dot{\varepsilon} = 10 \cdot 10^{-3}\ s^{-1}$. The course of the electrical resistance is qualitatively identical to that determined at the strain rate of $\dot{\varepsilon} = 0.1 \cdot 10^{-3}\ s^{-1}$. The only difference is in the strain level, at which it transforms into an exponential gradient (1.3% instead of 1.0%). The course of the AE in the range of $\varepsilon_t \approx 0$ to 0.8% however, correlated neither with R nor with AE, corresponding to $\dot{\varepsilon} = 0.1 \cdot 10^{-3}\ s^{-1}$.

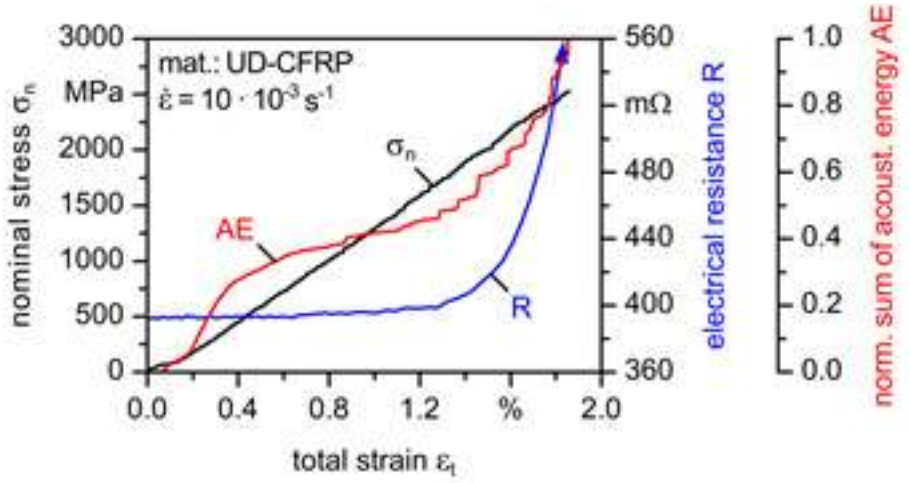

Figure 5. Quasi-static tensile test at $\dot{\varepsilon} = 10 \cdot 10^{-3}\ s^{-1}$

For a detailed description of the progression of the nominal sum of acoustic energy AE and for comparison with the results plotted in Fig. 3, the curves of AE for $\dot{\varepsilon} = 0.1 \cdot 10^{-3}\ s^{-1}$ and $\dot{\varepsilon} = 10 \cdot 10^{-3}\ s^{-1}$ are both presented in Fig. 6. It is evident that the AE in the case of $\dot{\varepsilon} = 10 \cdot 10^{-3}\ s^{-1}$ reaches up to approximately 40% of the total energy sum directly after the start of the tensile test until $\varepsilon_t \approx 1.0\%$. This increase is due to the summation of many signals with small individual energies (< 100). In contrast, in the case of $\dot{\varepsilon} = 0.1 \cdot 10^{-3}\ s^{-1}$, no measurable signals are detected at the start and, therefore, significant signals can only be detected after $\varepsilon_t \approx 1.0\%$. The difference in the signal progression can be analyzed in more detail from the process topography of HFIM (Fig. 7 (a-f)).

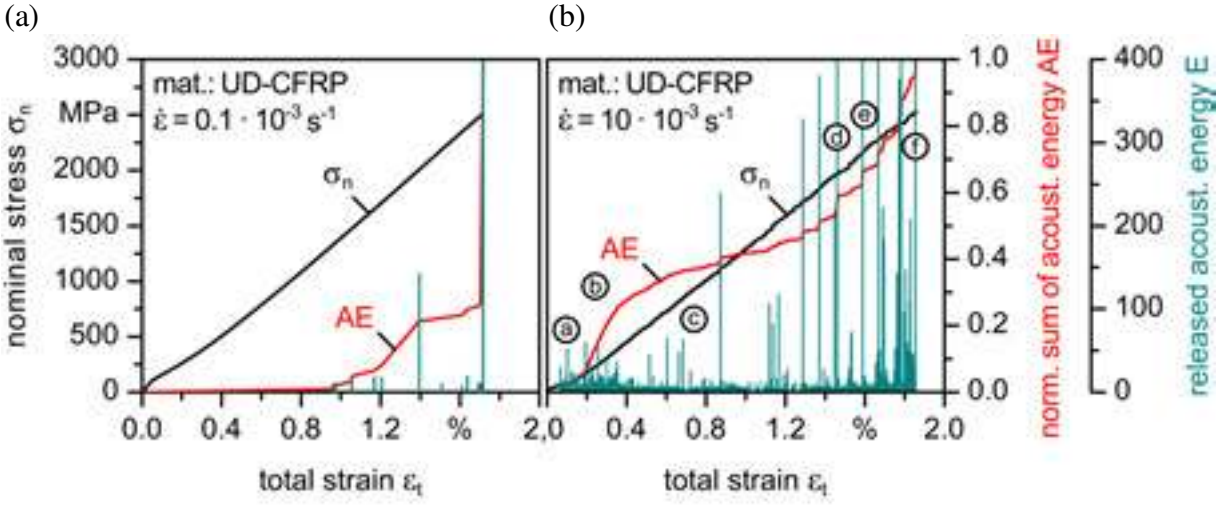

Figure 6. Progression of AE and E for $\varepsilon = 0.1 \cdot 10^{-3}\ s^{-1}$ (a) and $\varepsilon = 10 \cdot 10^{-3}\ s^{-1}$ (b)

The HFIM calculates the signals using a Fast Fourier Transformation (FFT) by fragmentation of the individual signals in the spectra and visualizes them simultaneously in the process topography. The process topography thus shows the detected acoustic signals of HFIM in real

time. They are represented by the amplitude (y-axis) and frequency spectra (z-axis) over time (x-axis). Figure 7 shows the exemplary graphics of the process topography at the selected strain conditions (a-f) during the tensile test at $\dot{\varepsilon} = 10 \cdot 10^{-3}\ s^{-1}$. No signal is detected until $\varepsilon_t = 0.1\%$. Signals of different energy levels are detected until $\varepsilon_t = 1.1\%$, but represent the similar characteristics. These signals, in comparison with the signals at high total strain, show small frequency spectrum and small energy amplitude. Both parameters are relevant characteristics for determination of damage mechanisms. Figure 7 (e) shows a significant change in signal characteristics, which continue until failure (Fig. 7 (f)). These signals show higher energy amplitude and an extended frequency spectrum, later being an indicator of impending damage, as the fibre cracks. This is confirmed by the progression of electrical resistance to a higher level before fibre fracture. The differing progression of the nominal sum of AE and R, in particular when $\varepsilon_t < 0.80\%$, due to the increase of the AE at almost constant electric resistance R indicates the detection of damage to the matrix. This hypothesis is reinforced by the low energies and low frequency spectrum of the detected signals in $\varepsilon_t < 0.80\%$.

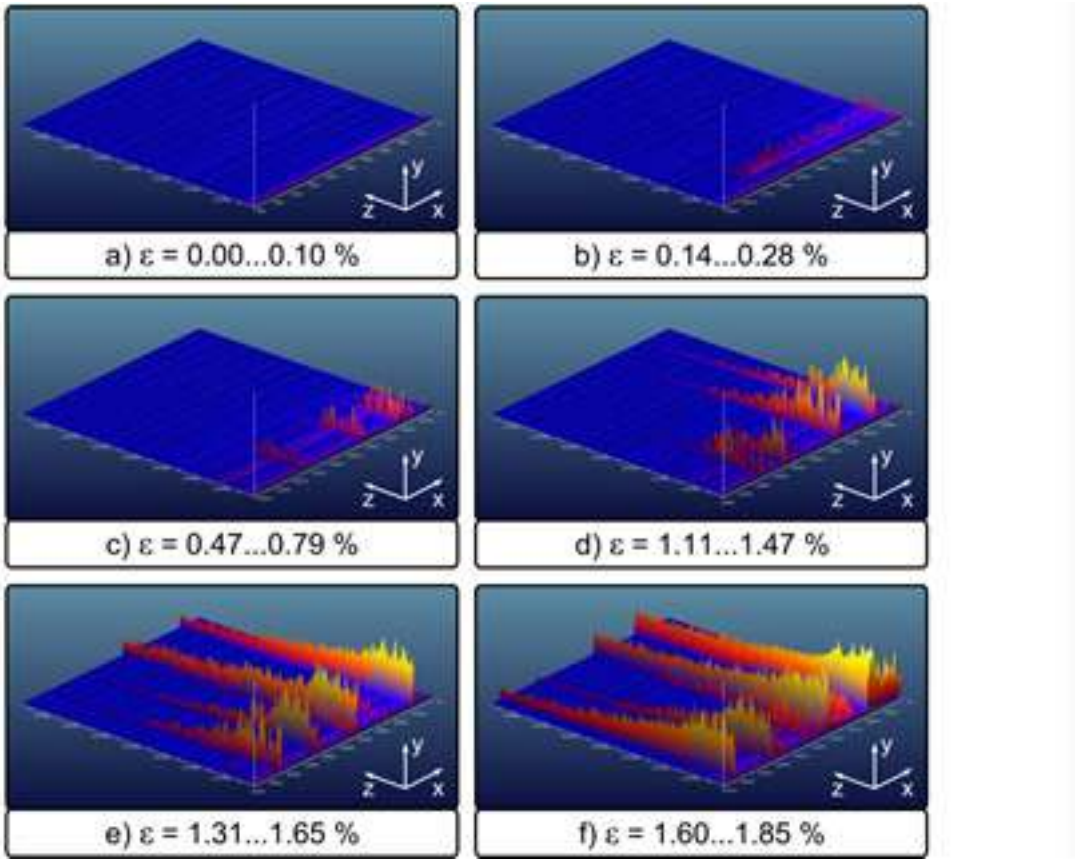

Figure 7. Process topography of HFIM for different strain conditions (a–f)

By considering the energy amplitude and frequency signals within the process topography, these hypotheses can be analyzed in detail with reliability. The combined use of HFIM and ERM allows the separation of the damage mechanisms and the association between matrix and the fibers at different stages of the tensile test by varying the strain rate.

4.2 Cyclic Tests

With the information available from the quasi-static tests, e.g. the correlation between R and AE as well as the knowledge about the HFIM signal evolution, cyclic multiple step tests were carried out to explore their potential for an efficient estimation of fatigue strength, to be validated by constant amplitude tests. Figure 8 shows the results of two stress-controlled multiple step tests with varied step lengths ΔN. The maximum stress $\sigma_{max,}$ the electrical resistance R and the nominal sum of acoustic emissions AE for UD-CFRP are displayed as a function of number of load cycles N. Step length ΔN was varied between 10^4 and 10^3 cycles per load sequence in order to investigate the influence of step length on the material's response parameters, so as to determine the possibility of reducing experimental effort. The response parameters are considered as measures of the damage state of the material and have been used as an indicator of fatigue strength.

Looking at Fig. 8 (a), having a step length of $\Delta N = 10^4$, two distinct areas can be recognized in the curve of the electrical resistance R. The value for the resistance remains constant for maximum stress values from 100 up to 900 MPa. Higher maximum stress values lead to an exponential increase in R until fracture at 1,300 MPa. The AE curve shows similar behaviour. Except for one signal step at 700 MPa, the progression of the curve is nearly identical to that of R. At first sight it seems as if the results for $\Delta N = 10^3$ (Fig. 8 (b)) differ from those in Fig. 8 (a). But the general shape of the curves is similar. There is also a constant value of R for $\sigma_{max} <$ 900-1,000 MPa, after which it experiences an exponential increase until fracture. In contrast to $\Delta N = 10^4$, the slope of the exponential increase is less, which leads to a higher fracture stress of 1,500 MPa. The curve of AE in Figure 8 (b) shows approximately the same progression as in Fig. 8 (a). The AE remains constant until $\sigma_{max} = 1{,}000$ MPa and undergoes an exponential increase afterwards.

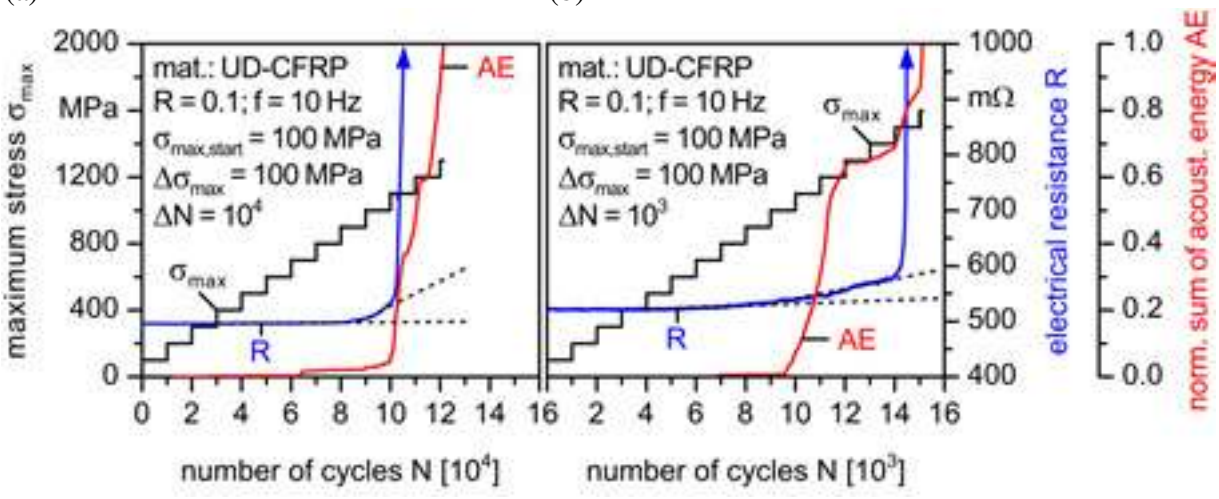

Figure 8. Multiple step tests with step length (a) 10^4 and (b) 10^3 load cycles

Taking the average of three tests for each step length, the specimen failure occurs at $\sigma_{max} = 1{,}400 \pm 265$ MPa for $\Delta N = 10^4$ cycles and $1{,}467 \pm 152$ MPa for $\Delta N = 10^3$ cycles, respectively. To derive an estimation of the fatigue strength at $N = 2 \cdot 10^6$ cycles, equivalent to the procedure used for many metallic materials, asymptotic lines were fitted to the slope of the AE and ERM curves, in order to identify the stress amplitude, which causes a significant change in material's reaction leading afterwards to exponential increase, cf. [6,7,8]. With respect to this, the exponential AE increase in Fig. 8 (b) is the earliest indication of fatigue failure after $N = 9.5 \cdot 10^3$ cycles. Both tests depicted in Fig. 8 result in an estimated fatigue strength of between 900 and 1,000 MPa. On average, the evaluation of three tests result in an

estimated fatigue strength of 1.000 ± 100 MPa ($\Delta N = 10^4$) and 1.033 ± 45 MPa ($\Delta N = 10^3$). The small difference between the two values can be justified by the shorter loading duration of the specimens at $\Delta N = 10^3$. In this case the specimen can reach higher stress amplitudes, due to smaller accumulated fatigue damage. However, the difference in results of the two test procedures is relatively small.

It appears that the combined evaluation of R and AE is a promising approach to determine the load step corresponding to the fatigue strength. Because of the linear-exponential shape of the curve for R in case of $\Delta N = 10^3$, estimation of the fatigue strength is difficult based only on R. Here a further evaluation of the HFIM signal is necessary to achieve an exact determination of σ_{max}, which causes a significant material reaction. In order to validate the estimated fatigue strength derived from the multiple step tests, constant amplitude tests were conducted at different σ_{max} levels. The resulting fatigue life N_f is a function of the employed stress σ_{max}, as shown by the S-N curve depicted in Fig. 9 (a). This relation can be approximated by the Basquin power law. Figure 9 (b) indicates, that the experimentally determined values correlate well with the ones derived from Basquin equation. Thus an estimation of the fatigue strength, based on the results of HFIM and ERM measurements during multiple step test, leads to reproducible results for the fatigue life, as derived from conventional constant amplitude tests, which is confirmed by the high coefficient of determination ($R^2 \approx 0.98$).

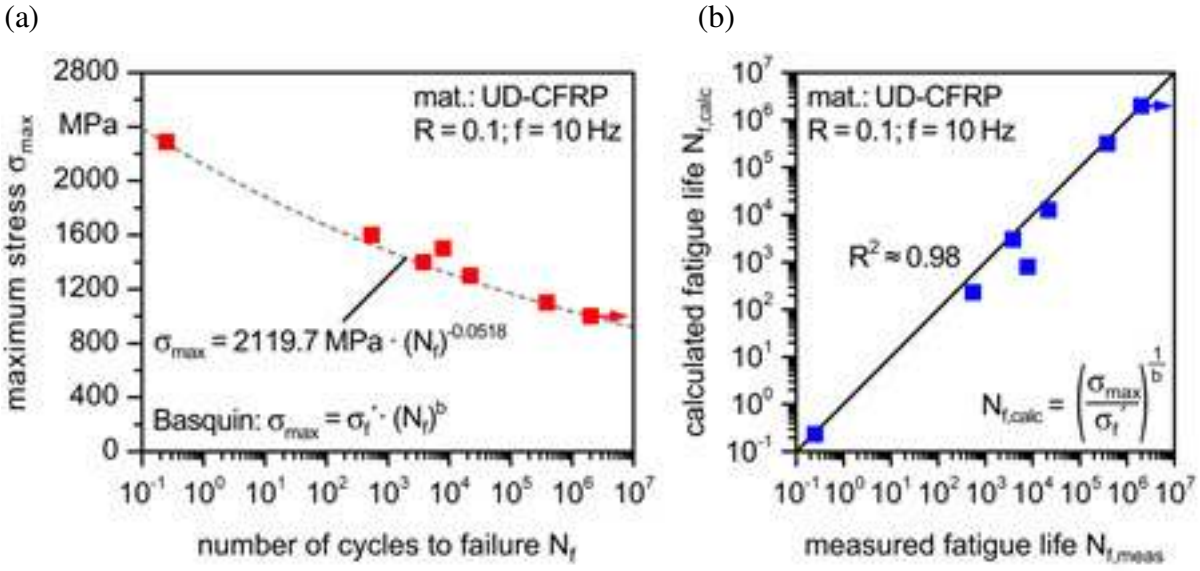

Figure 9. (a) Woehler curve as function of maximum stress versus number of cycles to failure, (b) Correlation between measured and calculated life time according to Basquin equation

5. Conclusions

The metrologically equipped experimental setup consisting of high frequency impulse measurement (HFIM) and electrical resistance measurement (ERM) allows the efficient determination of damage detection and evolution and the corresponding mechanisms as well as the estimation of the fatigue strength of CFRP. In tensile tests, the influence of strain rate on the HFIM waveform was determined. By combining the results of the HFIM, ERM and microstructural investigations, the fundamental damage mechanisms associated with the matrix and the carbon fibres were attributed, separated from each other and displayed on the stress-strain curve.

By using the combined measurement setup in multiple step tests, the fatigue properties were evaluated and the fatigue strength was estimated, which was successfully validated in constant amplitude fatigue tests. The variation of the step length in multiple step tests between 10^3 and 10^4 shows only a negligible effect on the estimated fatigue strength. So this method has a great potential for further reduction of time and cost expenditure in the context and to the advantage of industrial applications. The use of HFIM process to determine the damage mechanisms shows promising results. The analysis of the waveforms will be further intensified in order to clearly describe these damage mechanisms.

References

1 A B Strong 'Fundamentals of Composites Manufacturing: Materials, Methods and Applications', 2 ed., Dearborn, Michigan: Society of Manufacturing Engineers, 2008.

2. R Cuntze 'Auch Composites können ermüden!', Conference Carbon Composites, Session Engineering, Augsburg, 2012.

3. J Park, T Okabea, N Takeda, W Cutin 'Electromechanical modeling of unidirectional CFRP composites under tensile loading condition', Composites A: Applied Science and Manufacturing 33/2, pp. 267–275, 2002.

4. T Prasse, F Michel, G Mook, K Schulte and W. Bauhofer, 'A comparative investigation of electrical resistance and acoustic emission during cyclic loading of CFRP laminates', Composites Science and Technology, Vol 61, No 6, pp 831–835, 2001.

5. O Ceyson, M Salvia, L Vincent, 'Damage mechanism characterisation of carbon fibre / epoxy composite laminates by both electrical resistance measurements and acoustic emission analyses', Scripta Materialia, Vol 34, No 8 , pp 1273-1280, 1996.

6. F Walther 'Microstructure-oriented fatigue assessment of construction materials and joints using short-time load increase procedure', Materials Testing 56, 7-8, pp. 529–527, 2014.

7. F Walther, D Eifler 'Fatigue life calculation of SAE 1050 and SAE 1065 steel under random loading', International Journal of Fatigue 29, 9-11, pp. 1885-1892, 2007.

8. P Starke, F Walther, D Eifler 'Phybal - a short-time procedure for a reliable fatigue-life calculation', Advanced Engineering Materials 12, 4, pp. 276–282, 2010.

9. M Nakada, Y Miyano, M Kinoshita, R Koga, T Okuya and R Muki, 'Time-Temperature Dependence of Tensile Strength of Unidirectional CFRP', Journal of Composite Materials, Vol 36, No 22 , pp 2567-2581, 2002.

10. T Prasse, W Bauhofer, K Schulte, F. Michel, G. Mook 'In situ Schädigungsüberwachung von kohlenstofffaserverstärkten Kunststoffen mittels elektrischer Methoden', DGZfP-Conference, Zerstörungsfreie Materialüberwachung, Berlin, 2001.